2024 European Control Conference (ECC)
June 25-28, 2024. Stockholm, Sweden

Data-driven uncertainty propagation for stochastic predictive control of multi-energy systems

M. Batu Özmeteler[1,†], Deborah Bilgic[2,†,*], Guanru Pan[1], Alexander Koch[2], Timm Faulwasser[1]

***Abstract*— Stochastic predictive control schemes that account for epistemic and aleatoric uncertainties, i.e. lack of model knowledge and stochastic disturbances, are of major interest for multi-energy systems. However, there exists a trade-off between model complexity, computational effort, and accuracy of uncertainty quantification. This paper attempts to assess this trade-off by comparing a recently proposed approach combining Willems' fundamental lemma with polynomial chaos expansion to a model-based scheme that first propagates uncertainty with PCE and then considers chance constraints in the optimization. The simulation results show that the data-driven scheme yields similar performance and computational efficiency compared to the model-based scheme, with the advantage of avoiding the construction of explicit models.**

***Index Terms*— Data-driven control, Willems' fundamental lemma, polynomial chaos, uncertainty quantification, uncertainty propagation, multi-energy systems**

I. Introduction

As energy demand continues to rise and environmental regulations become more stringent, multi-energy systems, integrating several subsystems for different energy carriers, are gaining prominence. Data-driven control methods are of interest for such systems [1], [2]. In particular, data-driven predictive control based on the fundamental lemma by Willems *et al.* [3] is considered for multi-energy systems [4] and building control [5]. For recent reviews of applications of data-driven control, we refer to [6], [7].

The relevance of the fundamental lemma stems from the fact that it enables to represent the dynamics of Linear Time-Invariant (LTI) systems via prerecorded input and output data without the need for a parametric model. However, a major challenge for the control of multi-energy systems is to ensure reliable performance as the systems in question are subject to uncertainties. The recent paper [8] extends the fundamental lemma to stochastic systems using Polynomial Chaos Expansion (PCE), which enables efficient uncertainty quantification. In the literature, uncertainty is usually classified as either aleatoric—i.e., stemming from inherent randomness such as unpredictability of stochastic disturbances, eg., renewable generation throug wind of solar—or as epistemic—i.e., arising from incomplete model knowledge, e.g., parametric uncertainty. Several papers have used PCE, particularly for aleatoric uncertainty in the steady optimization of power systems [9].

The focus of the present paper is on the combination of data-driven control concepts with stochastic uncertainty descriptions of the energy demand. That is, we consider a setting with epistemic and aleatoric uncertainties. For this purpose, we adapt the stochastic data-driven predictive control framework from [8] for a sector-coupled energy system. Our contribution is the evaluation of the performance for the data-driven scheme through an extensive comparison to a model-based counterpart.

The remainder of the paper is structured as follows: in Section II, we recall the stochastic extension of the fundamental lemma. Section III presents the considered multi-energy system and introduces the considered stochastic model-based and data-driven predictive control approaches. Section IV compares both schemes. The paper concludes with summary and outlook in Section V.

Notation: Let $Z : \mathbb{I}_{[0,T-1]} \to \mathcal{L}^2(\Omega, \mathcal{F}, \mu; \mathbb{R}^{n_x})$ be a random vector-valued sequence with variables of dimension n_x, where the sample space is Ω, σ-algebra is $\mathcal{F}$, and the probability measure is μ. We denote the mean, variance and realization of Z as $\mathbb{E}[Z]$, $\mathbb{V}[Z]$, and $z \doteq Z(\omega) : \mathbb{I}_{[0,T-1]} \to \mathbb{R}^{n_x}$. The vectorization of z is given by $z_{[0,T-1]} \doteq [z_0^\top, z_1^\top, ..., z_{T-1}^\top]^\top$.

II. Preliminaries

We consider discrete-time systems of the form

$$X_{k+1} = AX_k + BU_k + EW_k, \quad X_0 = x_{\text{ini}}, \tag{1a}$$
$$Y_k = CX_k + DU_k + FW_k, \tag{1b}$$

with state $X_k \in \mathcal{L}^2(\Omega, \mathcal{F}_k, \mu; \mathbb{R}^{n_x})$, input $U_k \in \mathcal{L}^2(\Omega, \mathcal{F}_k, \mu; \mathbb{R}^{n_u})$, output $Y_k \in \mathcal{L}^2(\Omega, \mathcal{F}_k, \mu; \mathbb{R}^{n_y})$, and process disturbance $W_k \in \mathcal{L}^2(\Omega, \mathcal{F}_k, \mu; \mathbb{R}^{n_w})$. The σ-algebra $\mathcal{F}$ in the underlying filtered probability space $(\Omega, \mathcal{F}, (\mathcal{F}_k)_{k\in\mathbb{N}}, \mu)$ contains all available historical information. For the sake of simplicity and throughout the paper, the initial state $x_{\text{ini}} \in \mathbb{R}^{n_x}$ is assumed to be exactly known and the process disturbances W_k, $k \in \mathbb{N}$ are assumed to be independently distributed (non-i.i.d.) random variables, see also Remark 1 for details.

A. Basics of Polynomial Chaos Expansion

The main idea of PCE is that any random variable of finite variance is an element of an $\mathcal{L}^2(\Omega, \mathcal{F}, \mu; \mathbb{R})$ probability space which is spanned by an appropriate basis [10]. Specifically,

†: Equally contributing first authors, *: Corresponding author
[1]M. Batu Özmeteler, Guanru Pan and Timm Faulwasser are with Institute of Energy Systems, Energy Efficiency and Energy Economics, TU Dortmund University, 44227 Dortmund, Germany, and [2]Deborah Bilgic and Alexander Koch are with Corporate Research, Robert Bosch GmbH, 71272 Renningen, Germany, {batu.oezmeteler, guanru.pan} @tu-dortmund.de, {deborah.bilgic, alexander.koch3}@de.bosch.com, timm.faulwasser@ieee.org

an orthogonal polynomial basis $\{\phi^{\mathsf{j}}\}_{\mathsf{j}=0}^{\infty}$ is considered, which implies the orthogonality relation

$$\langle \phi^{\mathsf{i}}, \phi^{\mathsf{j}} \rangle = \int_{\Omega} \phi^{\mathsf{i}}(\omega)\phi^{\mathsf{j}}(\omega) d\mu(\omega) = \delta^{\mathsf{ij}} \langle \phi^{\mathsf{j}} \rangle^2, \tag{2}$$

where δ^{ij} is the Kronecker delta and $\langle \phi^{\mathsf{j}} \rangle^2 = \langle \phi^{\mathsf{j}}, \phi^{\mathsf{j}} \rangle$. The PCE of a real-valued random variable $Z \in \mathcal{L}^2(\Omega, \mathcal{F}, \mu; \mathbb{R})$ with respect to the basis $\{\phi^{\mathsf{j}}\}_{\mathsf{j}=0}^{\infty}$ is

$$Z = \textstyle\sum_{i=0}^{\infty} \ \mathsf{z}^{\mathsf{j}} \phi^{\mathsf{j}} \quad \text{with} \quad \mathsf{z}^{\mathsf{j}} = \big\langle Z, \ \phi^{\mathsf{j}} \big\rangle / \big\langle \phi^{\mathsf{j}} \big\rangle^2 \tag{3}$$

with $\mathsf{z}^{\mathsf{j}} \in \mathbb{R}$ as the j-th order PCE coefficient. The expectation and variance of Z can be determined by the PCE coefficients

$$\mathbb{E}[Z] = \mathsf{z}^{\mathsf{0}}, \quad \mathbb{V}[Z] = \textstyle\sum_{\mathsf{j}=1}^{L-1} (\mathsf{z}^{\mathsf{j}})^2 \langle \phi^{\mathsf{j}} \rangle^2, \tag{4}$$

where $(\mathsf{z}^{\mathsf{j}})^2 = \mathsf{z}^{\mathsf{j}} \circ \mathsf{z}^{\mathsf{j}}$ denotes the Hadamard product and L is the number of considered terms in the series. The $\mathcal{L}^2(\Omega, \mathcal{F}_k, \mu; \mathbb{R}^{n_z})$ nature of the random variables in (1) enables the expression of its trajectories in terms of the corresponding PCE coefficients. By replacing all random variables with their PCE representations in $\{\phi^{\mathsf{j}}\}_{\mathsf{j}=0}^{L-1}$ and performing Galerkin projection onto the basis functions ϕ^{j} [11], one obtains the dynamics of the PCE coefficients. With given $\mathsf{w}_k^{\mathsf{j}}, k \in \mathbb{N}$, this yields

$$\mathsf{x}_{k+1}^{\mathsf{j}} = A\mathsf{x}_k^{\mathsf{j}} + B\mathsf{u}_k^{\mathsf{j}} + E\mathsf{w}_k^{\mathsf{j}}, \quad \mathsf{x}_0^{\mathsf{j}} = \delta^{\mathsf{0j}} x_{\text{ini}}, \tag{5a}$$

$$\mathsf{y}_k^{\mathsf{j}} = C\mathsf{x}_k^{\mathsf{j}} + D\mathsf{u}_k^{\mathsf{j}} + F\mathsf{u}_k^{\mathsf{j}}. \tag{5b}$$

B. Stochastic Extension of the Fundamental Lemma

To construct a data-driven system representation based on Willems' fundamental lemma, we rely on the use of a persistently exciting input trajectory.

Definition 1 (Persistency of excitation [3]): A signal sequence $s_{[0,T-1]} \in \mathbb{R}^{n_s T}$ is said to be persistently exciting of order t where $t, T \in \mathbb{N}^+$ with $T \geq t(n_s + 1) - 1$, if the Hankel matrix $\mathscr{H}_t(s_{[0,T-1]}) \doteq \begin{bmatrix} s_0 & \cdots & s_{T-t} \\ \vdots & \ddots & \vdots \\ s_{t-1} & \cdots & s_{T-1} \end{bmatrix}$ is of full row rank.

Furthermore, the stochastic system (1) admits the following path-wise realization dynamics for a fixed disturbance sequence $w_k, k \in \mathbb{N}$

$$x_{k+1} = Ax_k + Bu_k + Ew_k, \quad x_0 = x_{\text{ini}}, \tag{6a}$$

$$y_k = Cx_k + Du_k + Fw_k. \tag{6b}$$

Assumption 1 (System assumptions and measurements): In (1) and (6), the pair $(A, [B, E])$ is controllable but the matrices A, B and E are unknown. Moreover, u_k, y_k, and w_{k-1} are considered to be measurable at instant k. □

The stochastic variant [8] of the fundamental lemma [3] demonstrates how the data of realization trajectories satisfying (6) can be used to represent (1).

Lemma 1 (Stochastic fundamental lemma [8]): Consider system (1), its random variable trajectories $(Y, U, W)_{[0,T-1]}$ and the corresponding realization trajectories $(y, u, w)_{[0,T-1]}$ from (5). Suppose $(u, w)_{[0,T-1]}$ is persistently exciting of order $n_x + N$ and let Assumption 1 hold. Then, $(Y, U, W)_{[0,N-1]}$ is an N-length trajectory of (1) if and only if there exists a random vector $G \in \mathcal{L}^2(\Omega, \mathcal{F}, \mu; \mathbb{R}^{T-N+1})$ such that

$$\mathscr{H}_N(z_{[0,T-1]})G = Z_{[0,N-1]}, \tag{7}$$

holds for all $(z, Z) \in \{(y, Y), (u, U), (w, W)\}$. □

The structural similarity in between (1), (5), and (6) allows to utilize a Hankel matrix of realizations to compute PCE coefficient trajectories.

Corollary 1 (PCE coefficients via realizations [8]): Let the conditions of Lemma 1 hold. Then, $(\mathsf{y}, \mathsf{u}, \mathsf{w})_{[0,N-1]}^{\mathsf{j}}$ is a trajectory of the dynamics of PCE coefficients from (5) if and only if there exists a $\mathsf{g}^{\mathsf{j}} \in \mathbb{R}^{T-N+1}$ such that

$$\mathscr{H}_t(z_{[0,T-1]})\mathsf{g}^{\mathsf{j}} = \mathsf{z}_{[0,N-1]}^{\mathsf{j}}, \quad \mathsf{j} \in \mathbb{I}_{[0,t-1]}, \tag{8}$$

holds for all $(z, \mathsf{z}) \in \{(y, \mathsf{y}), (u, \mathsf{u}), (w, \mathsf{w})\}$. □

III. Stochastic Optimal Control of a Multi-Energy Distribution System

A. Problem Statement

The main object of our investigations are multi-energy systems motivated by [12] with modifications sketched in [4]. The considered system comprises three components, namely, a Combined Heat and Power (CHP) engine, a boiler, and a Thermal Energy Storage (TES) that are connected through electrical and thermal grids. For the sake of simplicity, we refer to any specific component with the subscript $i \in \mathrm{I}$, $\mathrm{I} = \{\mathrm{CHP}, \mathrm{BO}, \mathrm{TES}\}$ and to the underlying grids with the subscript $s \in \mathrm{S}$, $\mathrm{S} = \{\mathrm{TG}, \mathrm{EG}\}$. In addition, we denote heat and power flow with $\mathcal{Q}, \mathcal{P}$ [kW] and use $\mathcal{E}$ [kWh] to represent the amount of stored energy. Figure 1 illustrates the energy flows and the modelling of the multi-energy system along with its states, control inputs, and outputs, cf. the summary in Table I. For the outputs of the components y, we consider Gaussian distributed measurement noise.

The working principle of the system is as follows: The energy supplies gas ($\mathcal{Q}_{\mathrm{CHP}}^{\mathrm{in}}, \mathcal{Q}_{\mathrm{BO}}^{\mathrm{in}}$) and electricity ($\mathcal{P}_{\mathrm{EG}}^{\mathrm{in}}, \mathcal{P}_{\mathrm{PV}}^{\mathrm{OB}}, \mathcal{P}_{\mathrm{PV}}^{\mathrm{EF}}$) from the corresponding grids and Photovoltaic (PV) units. The CHP engine generates heat ($\mathcal{Q}_{\mathrm{CHP}}^{\mathrm{out}}$) and electricity ($\mathcal{P}_{\mathrm{CHP}}^{\mathrm{out}}$) simultaneously while the boiler produces only heat ($\mathcal{Q}_{\mathrm{BO}}^{\mathrm{out}}$) from the gas supply. The thermal and electrical grids distribute energy according to the instantaneous demands ($\mathcal{Q}_{\mathrm{dem}}, \mathcal{P}_{\mathrm{dem}}$). Excess heat is initially stored in TES. If the amount of excess heat surpasses the TES capacity or if the generated heat is insufficient, this imbalance is compensated for by the thermal grid ($\mathcal{Q}_{\mathrm{TG}}$). The excess power ($\mathcal{P}_{\mathrm{EG}}^{\mathrm{out}}$) is sold back to the electricity grid, while in case of lack of power ($\mathcal{P}_{\mathrm{EG}}^{\mathrm{in}}$) is purchased.

In the following, we only outline crucial aspects of modelling the system components. We refer to [4], [12] for further details. The dynamics of CHP and boiler are determined by thermal efficiency curves η_i^{heat} which depend nonlinearly on the associated load fractions

$$\frac{\mathrm{d}}{\mathrm{dt}}\lambda_{\mathsf{i}} = \frac{1}{\tau_i}\left(\eta_{\mathsf{i}}^{\mathrm{heat}}(\lambda_{\mathsf{i}})\frac{\mathcal{Q}_{\mathsf{i}}^{\mathrm{in}}}{\mathcal{Q}_{\mathsf{i}}^{\mathrm{nom}}} - \lambda_{\mathsf{i}}\right), \quad \forall \mathsf{i} \in \{\mathrm{CHP}, \mathrm{BO}\}, \tag{9}$$

where $\mathcal{Q}_{\mathsf{i}}^{\mathrm{nom}}$ is set to 496.3 kW and 530 kW for CHP and boiler units, respectively. As the thermal efficiencies are

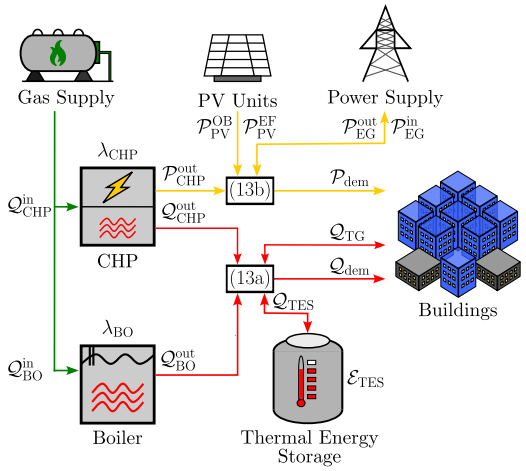

Fig. 1. The considered multi-energy system [12]

discontinuous with a dead band for low load fractions, boiler and CHP models utilize adapted smooth efficiencies [4], [12]. The outputs for both components are

$$\mathcal{Q}_{\text{CHP}}^{\text{out}} = \mathcal{Q}_{\text{CHP}}^{\text{nom}} \lambda_{\text{CHP}}, \quad \mathcal{P}_{\text{CHP}}^{\text{out}} = \eta_{\text{CHP}}^{\text{el}}(\lambda_{\text{CHP}}) \mathcal{Q}_{\text{CHP}}^{\text{in}}, \tag{10}$$

$$\mathcal{Q}_{\text{BO}}^{\text{out}} = \mathcal{Q}_{\text{BO}}^{\text{nom}} \lambda_{\text{BO}} \tag{11}$$

where $\eta_{\text{CHP}}^{\text{el}}$ is the smoothened power efficiency of CHP engine. The simple TES model is given by

$$\frac{\mathrm{d}}{\mathrm{dt}} \mathcal{E}_{\text{TES}} = \mathcal{Q}_{\text{TES}} - \frac{1}{\tau_{\text{loss}}} \mathcal{E}_{\text{TES}} \tag{12}$$

with $\tau_{\text{loss}} = 200$ the time constant for heat loss. The thermal and electrical power balances read

$$\mathcal{Q}_{\text{TES}} = \mathcal{Q}_{\text{CHP}}^{\text{out}} + \mathcal{Q}_{\text{BO}}^{\text{out}} - \mathcal{Q}_{\text{dem}} - \mathcal{Q}_{\text{TG}}, \tag{13a}$$

$$\mathcal{P}_{\text{EG}}^{\text{out}} = \mathcal{P}_{\text{PV}}^{\text{EF}} + \mathcal{P}_{\text{PV}}^{\text{OB}} + \mathcal{P}_{\text{EG}}^{\text{in}} + \mathcal{P}_{\text{CHP}}^{\text{out}} - \mathcal{P}_{\text{dem}}. \tag{13b}$$

Due to the coupling expressed by (13) , the operation of the system is influenced by disturbances, i.e., by the thermal demand and the power demand $\mathcal{Q}_{\text{dem}}, \mathcal{P}_{\text{dem}}$ as well as by the renewable generations $\mathcal{P}_{\text{PV}}^{\text{OB}}, \mathcal{P}_{\text{PV}}^{\text{EF}}$. In this work, we are specifically interested in accounting for the variability of $\mathcal{Q}_{\text{dem}}$ and tthe associated risks for the operation of the TES. Hence, we assume that all other disturbances except for the thermal demand follow a fixed sequence of realizations (i.e. a scenario). Specifically, due to (13a), the uncertainty of future predictions of $\mathcal{Q}_{\text{dem}}$ propagates to $\mathcal{Q}_{\text{TES}}$ and thereby renders the underlying dynamics of stored thermal energy $\mathcal{E}_{\text{TES}}$ stochastic. To account for this, we design two *stochastic* predictive control schemes in the next section.

Remark 1 (Forecasting by Gaussian Processes): To forecast future thermal demand $\mathcal{Q}_{\text{dem}}$ and its statistical properties, we utilize Gaussian Processes (GPs). Specifically, with a prior mean function $m_{\text{prior}}(t)$ trained on historical data and a squared exponential kernel $k(l, \theta)$ determined by hyperparameters of length scale l and signal variance θ, we denote a trained GP by $\mathcal{GP}(m_{\text{prior}}(t), k(l, \theta))$. Within each instant of our numerical simulations, the last n_{obs} observed instances of $\mathcal{Q}_{\text{dem}}$ are used to retrain the hyperparameters by

TABLE I

System variables for components and grids

Element	States x	Inputs u	Outputs y	Disturbances w
CHP	λ_{CHP}	$\mathcal{Q}_{\text{CHP}}^{\text{in}}$	$[\mathcal{Q}_{\text{CHP}}^{\text{out}}, \mathcal{P}_{\text{CHP}}^{\text{out}}]^\top$	-
BO	λ_{BO}	$\mathcal{Q}_{\text{BO}}^{\text{in}}$	$\mathcal{Q}_{\text{BO}}^{\text{out}}$	-
TES	$\mathcal{E}_{\text{TES}}$	$\mathcal{Q}_{\text{TES}}$	$\mathcal{E}_{\text{TES}}$	-
TG	-	-	$\mathcal{Q}_{\text{TG}}$	$\mathcal{Q}_{\text{dem}}$
EG	-	-	$[\mathcal{P}_{\text{EG}}^{\text{in}}, \mathcal{P}_{\text{EG}}^{\text{out}}]^\top$	$[\mathcal{P}_{\text{dem}}, \mathcal{P}_{\text{PV}}^{\text{OB}}, \mathcal{P}_{\text{PV}}^{\text{EF}}]^\top$

maximizing the log-marginal likelihood of the GP. The prior mean function $m_{\text{prior}}(t)$ is refitted by taking into account the respective deviations of the sampled realizations of $\mathcal{Q}_{\text{dem}}$ from the initial prior mean to obtain the posterior mean $m_{\text{post}}(t)$. Moreover with the resulting standard deviations $\sigma(t)$, we consider the forecasting of $\mathcal{Q}_{\text{dem},k}$ at $t = k\delta_t$ as

$$\mathcal{Q}_{\text{dem},k} = m_{\text{post}}(k\delta_t) + \sigma(k\delta_t)\xi_k \tag{14}$$

with $\xi_k \sim \mathcal{N}(0,1)$ as independent standard Gaussian distributions. Note that due to the time-varying nature of the mean and standard deviation (the latter implies a shift in variance), we have a non-i.i.d. setting for the disturbance. The technical specifications for the considered GPs are detailed in Section IV-A. □

Remark 2 (Construction of PCE basis): If suitable polynomial bases are chosen [8] stochastic uncertainty that adheres to frequently used distributions allows for exact PCE representations with finitely many terms. Since $\mathcal{Q}_{\text{dem},k}$, $k \in \mathbb{I}_{[0,N-1]}$, are independent Gaussians (14), we construct the finite-dimensional basis

$$\{\phi^j\}_{j=0}^{N} = \{1, \xi_0, ..., \xi_{N-1}\}. \tag{15}$$

which collects all stochastic uncertainties and allows exact PCE representations involved in (1) [8]. □

Remark 3 (Separation of prediction horizons): A limitation of PCE regarding aleatoric uncertainties is its linear growth in the number of basis functions over the prediction horizon. To address this, we propagate the uncertainty for an initial segment of the horizon and subsequently we consider only the mean information. Specifically, we separate the prediction horizon $[0, 1, ..., N-1]$ into two parts $[0, ..., N_1 - 1]$ and $[N_1, ..., N-1]$ whereby the latter considers $N_2 = N - N_1$ time steps. During the first phase $[0, ..., N_1 - 1]$, the uncertain thermal demands $\mathcal{Q}_{\text{dem}}$ admit the parametrization (14) which allows the propagation of means and standard deviations for system variables. During the second phase $[0, ..., N-1]$ only the mean-value forecast of $\mathcal{Q}_{\text{dem}}$ is considered. □

B. Model-based and Data-driven Predictive Control

In this section, we formulate model-based and data-driven OCPs with the control objective of meeting energy demands while minimizing the total operational cost of our sector-coupled energy system. We address the problem described in Section III-A by quantifying the uncertainty affiliated with y_{TES} to a sufficient degree and accounting for its influence by

TABLE II
Comparison of algorithms

Scheme	Uncertainty Propagation	Convexity	Comments on Application
Model-based	via forward propagation, prior to OCP	non-convex	only for Gaussian RVs and LTI systems
Data-driven	implicitly via PCE coefficients within the OCP	convex	applicable to non-Gaussian RVs

employing chance constraints. To facilitate comparison, Table II summarizes main aspects of the proposed algorithms.

1) Model-based OCP: We implement uncertainty propagation only for the TES as a step external to the optimization which then allows to formulate chance constraints in the OCP. Specifically, we leverage PCE to propagate the uncertainty arising due to $\mathcal{Q}_{\text{dem}}$ through the dynamics of TES prior to the solution of our OCP. We consider the following OCP at instance $k \in \mathbb{N}$ with horizon $N \in \mathbb{N}^+$

$$\min_{\substack{u_i, y_i \\ x_i, s_{\text{TG}}}} \sum_{i \in \text{I}} \sum_{k=0}^{N-1} \ell_i(u_{i,k}, y_{i,k}, y_{\text{EG},k}) + \lambda_s \|s_{\text{TG}}\|_2^2 \quad (16a)$$

s.t. for all $i \in \text{I},\ k \in \mathbb{I}_{[0,N-1]}$:

$$x_{i,k+1} = f_i(x_{i,k},\ u_{i,k}), \quad x_{i,0} = x_i^{\text{ini}} \quad (16b)$$

$$y_{i,k} = h_i(x_{i,k},\ u_{i,k}) \quad (16c)$$

$$u_{\text{TES},k} = y_{\text{CHP},k} + y_{\text{BO},k} - \bar{w}_{\text{TG},k} - s_{\text{TG},k} \quad (16d)$$

$$0 = c_1^\top y_{\text{EG},k} + c_2^\top \bar{w}_{\text{EG},k} \quad (16e)$$

$$u_{i,k} \in \mathbb{U}_i, \quad (16f)$$

$$\underline{y_{\text{TES}}} + \beta(\epsilon)\, \hat{\sigma}_{y_{\text{TES},k}} \leq y_{\text{TES},k} \leq \overline{y_{\text{TES}}} - \beta(\epsilon)\, \hat{\sigma}_{y_{\text{TES},k}} \quad (16g)$$

where (16b) and (16c) collect all state and output equations of the system components, which are described by the equations (9)-(12). Note that the component dynamics do not include any disturbance, cf. Table I. The stage cost in (16a) reads $\ell(u_{i,k}, y_{i,k}, y_{\text{EG},k}) = \ell_{\text{cost}} + \ell_{\text{reg}}$ with

$$\ell_{\text{cost}} = p_{\text{gas}}^{\text{buy}}(u_{\text{CHP},k} + u_{\text{BO},k}) + [p_{\text{el}}^{\text{buy}}, -p_{\text{el}}^{\text{sell}}] y_{\text{EG}}, \quad (17a)$$

$$\ell_{\text{reg}} = \gamma_{\text{CHP}} {u_{\text{CHP},k}}^2 + \gamma_{\text{BO}} {u_{\text{BO},k}}^2 + \gamma_{\text{TES}} {u_{\text{TES},k}}^2, \quad (17b)$$

where $p_{\text{gas}}^{\text{buy}}$ is the buying price of gas, $p_{\text{el}}^{\text{buy}}, p_{\text{el}}^{\text{sell}}$ are the buying and selling prices of electricity respectively. Equation (17a) penalizes the control inputs weighted by the relevant prices and (17b) includes a squared term for the control inputs multiplied with regularization weighting factors γ_{CHP}, γ_{BO} and γ_{TES}.

For all time steps $k \in \mathbb{I}_{[0,N-1]}$, the power balance equations (13a) and (13b) are considered in (16d), (16e) where $s_{\text{TG},k}$ refers to $\mathcal{Q}_{\text{TG}}$, which, from the optimization point of view, is a slack variable introduced to compensate for the violation of the thermal power balance due to inaccurate prediction of thermal demand. This is similar to the concept of a slack bus in power systems [9] and hence this slack variable is penalized in the objective. Furthermore, $\bar{w}_{\text{TG},k}$ contains the forecasted mean of the thermal demand $\mathcal{Q}_{\text{dem}}$ and $\bar{w}_{\text{EG},k}$ is a vector of forecasted means of power demand and renewable generations with $c_1 = [1, -1]^\top,\ c_2 = [-1, 1, 1]^\top$. The input constraints (16f) reflect operational limits.

In the following, we explain how the uncertainty propagation is performed in the model-based scheme. PCE proves to be a suitable tool for this purpose as the linearity of the TES model can be exploited. In view of the remarks from Section II, it is possible to replace the dynamics of any stochastic LTI system of the form (1) with equivalent PCE coefficient dynamics (5), and thus acheive exact forward propagation. To this end, we first rewrite the TES model (12) to fit the generic notation from (1). We substitute (13a) into (12), and we discretize the resulting ODE with δ_t to obtain

$$X_{\text{TES},k+1} = A_d X_{\text{TES},k} + B_d \tilde{u}_{\text{TES},k} + E_d W_{\text{TES},k},$$
$$Y_{\text{TES},k} = C_d X_{\text{TES},k}$$

where $A_d = 1 - (\delta_t/\tau_{\text{loss}})$, $B_d = \delta_t$, $C_d = 1$, $E_d = -\delta_t$. Accordingly, we split the model input $\mathcal{Q}_{\text{TES}}$ into two parts. We have $(\mathcal{Q}_{\text{CHP}}^{\text{out}} + \mathcal{Q}_{\text{BO}}^{\text{out}} - \mathcal{Q}_{TG})$ as the new input $\tilde{u}_{\text{TES},k}$ and $\mathcal{Q}_{\text{dem}}$ as the exogenous disturbance $w_{\text{TES},k}$. Particularly, we assume $\tilde{u}_{\text{TES},k}$ to be deterministic within this context. Next, we express $\mathcal{Q}_{\text{dem}}$ in its PCE representation (14) as explained in Remark 1, and adjust its parametrization according to the separation of our prediction horizon $[0, 1, ..., N-1]$ into phases $[0, 1, ..., N_1 - 1]$ and $[N_1, ..., N-1]$, cf. Remark 3. Relying on (5), we compute the PCE coefficients of y_{TES} at every instant on the initial phase and we determine the corresponding standard deviations via (4). Throughout the second phase, the predicted standard deviations stay constant until the end of the horizon. Subsequently in (16g), chance constraints are formulated by means of the corresponding Chebyshev-Cantelli inequality where $\underline{y_{\text{TES}}}$, $\overline{y_{\text{TES}}}$ are the lower and upper bounds of y_{TES}, $\hat{\sigma}_{y_{\text{TES},k}}$ is the estimated standard deviation of y_{TES} at instance k, and $\beta(\epsilon) = \sqrt{(1-\epsilon)/\epsilon}$ with $\epsilon \in [0, 1)$ as the confidence value [13].

2) Data-driven OCP: The considered data-driven predictive control approach assumes a stochastic disposition for the complete system and reshapes the dynamics in (16b), (16c) into a PCE-based, data-driven representation. Exploiting Lemma 1 and Corollary 1 we utilize recorded input-output realization data to predict the corresponding PCE coefficient trajectories. To this end, we represent all disturbances in the respective PCE basis (14) and we consider the basis (15) from Remark 2 for the system inputs and outputs to achieve exact PCE representations. The stochastic data-driven reformulation of (16) reads

$$\min_{\substack{\mathsf{g}, \mathsf{u}, \mathsf{y} \\ \sigma, \mathsf{s}_{\text{TG}}}} \sum_{i \in \text{I}} \left(\sum_{k=0}^{N-1} \ell_i(\mathsf{u}_{i,k}^0, \mathsf{y}_{i,k}^0, \mathsf{y}_{\text{EG},k}^0) + r_i(\mathsf{g}_i^{\mathsf{j}}, \sigma_i^{\mathsf{j}}, \mathsf{s}_{\text{TG}}^{\mathsf{j}}) \right) \quad (18a)$$

s.t. for all $i \in \text{I},\ \mathsf{j} \in \mathbb{I}_{[0,L-1]},\ k \in \mathbb{I}_{[0,N-1]}$,

$$\begin{bmatrix} \mathscr{H}_{N+T_i^{\text{ini}}}(u_{i[0,T_i-1]}) \\ \mathscr{H}_{N+T_i^{\text{ini}}}(y_{i[0,T_i-1]}) \end{bmatrix} \mathsf{g}_i^{\mathsf{j}} = \begin{bmatrix} \mathsf{u}_{i[-T_i^{\text{ini}},N-1]}^{\mathsf{j}} \\ \mathsf{y}_{i[-T_i^{\text{ini}},N-1]}^{\mathsf{j}} \end{bmatrix}, \quad (18b)$$

$$\mathsf{u}_{\text{TES},k}^{\mathsf{j}} = \mathsf{y}_{\text{CHP},k}^{\mathsf{j}} + \mathsf{y}_{\text{BO},k}^{\mathsf{j}} - \mathsf{w}_{\text{TG},k}^{\mathsf{j}} - \mathsf{s}_{\text{TG},k}^{\mathsf{j}} \quad (18c)$$

$$0 = c_1^\top \mathsf{y}_{\text{EG},k}^{\mathsf{j}} + c_2^\top \bar{\mathsf{w}}_{\text{EG},k}^{\mathsf{j}} \quad (18d)$$

$$\underline{y_{\text{TES}}} \leq \mathsf{y}^{0}_{\text{TES},k} \pm \sqrt{\theta(\epsilon) \sum_{\mathsf{j}=1}^{L-1} (\mathsf{y}^{\mathsf{j}}_{\text{TES},k})^2 \langle \phi \mathsf{j} \rangle^2} \leq \overline{y_{\text{TES}}}, \quad (18e)$$

$$\mathsf{u}^{\mathsf{j}^{'}}_{i,k} = 0, \forall \mathsf{j}^{'} \in \mathbb{I}_{[(k+1)(L_w-1)+1,\ L-1]}, \quad (18f)$$

$$\begin{aligned} \mathsf{u}^{\mathsf{j}}_{[-T_i^{\text{ini}},-1]} &= \tilde{\mathsf{u}}^{\mathsf{j}}_{[-T_i^{\text{ini}},-1]}, \\ \mathsf{y}^{\mathsf{j}}_{[-T_i^{\text{ini}},-1]} &= \tilde{\mathsf{y}}^{\mathsf{j}}_{[-T_i^{\text{ini}},-1]} + \sigma_i^{\mathsf{j}}, \end{aligned} \quad (18g)$$

where the PCE coefficient dynamics of each system component are described by (18b) with T_i^{ini} being the length of past system measurements. T_i stands for the length of recorded realization trajectories of inputs and outputs where inputs are persistently exciting of order $n_{x_i} + N + T_i^{\text{ini}}$. OCP (18) above and its model-based counterpart (16) share several commonalities. To avoid redundant explanations, we only elaborate on the aspects where (18) differs from (16).

In (18), PCE coefficients of inputs $\mathsf{u}^{\mathsf{j}}_{i[-T_i^{\text{ini}},N-1]} \in \mathbb{R}^{Nn_{u_i}}$, outputs $\mathsf{y}^{\mathsf{j}}_{i[-T_i^{\text{ini}},N-1]} \in \mathbb{R}^{Nn_{y_i}}$, electrical grid inputs $u^{\mathsf{j}}_{\text{EG},k} \in \mathbb{R}^{Nn_{u_{\text{EG}}}}$, outputs $y^{\mathsf{j}}_{\text{EG},k} \in \mathbb{R}^{Nn_{y_{\text{EG}}}}$, column space selectors $\mathsf{g}^{\mathsf{j}}_i \in \mathbb{R}^{T_i-N-T_i^{\text{ini}}+1}$ and slack variables $\sigma^{\mathsf{j}}_i \in \mathbb{R}^{Nn_{y_i}}$, $\mathsf{s}^{\mathsf{j}}_{\text{TG}} \in \mathbb{R}^{N}$ are the decision variables. The initial condition specified with $\tilde{\mathsf{y}}^{\mathsf{j}}_{[-T_i^{\text{ini}},-1]}$ in (18g) is measured and $\tilde{\mathsf{u}}^{\mathsf{j}}_{[-T_i^{\text{ini}},-1]}$ is assumed to be known through measurements.

The cost function (18a) relies on the linear (economic) stage cost (17a) with first-order PCE coefficients (i.e. mean values) of system inputs and outputs as its arguments. Put differently, it is the expected operation cost. Moreover, it entails the regularization term

$$r_i(\mathsf{g}^{\mathsf{j}}_i, \sigma^{\mathsf{j}}_i, \mathsf{s}^{\mathsf{j}}_{\text{TG}}) = \sum_{\mathsf{j}=0}^{L-1} \lambda_{\mathsf{g}} \|\mathsf{g}^{\mathsf{j}}_i\|_1 + \lambda_{\sigma} \|\sigma^{\mathsf{j}}_i\|_1 + \lambda_{\mathsf{s}} \|\mathsf{s}^{\mathsf{j}}_{\text{TG}}\|_2^2,$$

where $\lambda_{g^{\mathsf{j}}}, \lambda_{\sigma}, \lambda_s$ are user-defined penalties for $\mathsf{g}^{\mathsf{j}}_i$, σ_i. The slack variables g^{j} and σ^{j} compensate for plant-model mismatch and measurement noise via (18g). We refer to [14] for similar regularization. The slack variable $\mathsf{s}^{\mathsf{j}}_{\text{TG}}$ renders the power balance (18c) feasible. With the addition of the slack variables, the risk of infeasibility occurring in closed-loop is alleviated.

With constraint (18e), we restate (16g) in terms of PCE coefficients and to preserve the convexity of the OCP, we reformulate the arising second-order cone constraints according to [15]. Additionally, (18f) is imposed on the PCE coefficients of the inputs to ensure causality properties of the computed solution. This constraint can also be understood as parameterizing the stochastic inputs U_i as an affine causal (disturbance) policy similar to [16], in which the current input depends on the knowledge of current and past disturbance realizations. Therefore, the applied control input in closed loop has the following form

$$u_{i,0} = \mathsf{u}^{0,\star}_{i,0} + \mathsf{u}^{1,\star}_{i,0} \xi_0(\omega) \quad (19)$$

with $\xi_0(\omega) = (\mathcal{Q}_{\text{dem},0}(\omega) - \mu_{\mathcal{Q}_{\text{dem},0}})/\sigma_{\mathcal{Q}_{\text{dem},0}}$.

TABLE III
Specifications of Gaussian processes

Gaussian Process	**Length Scale** l Initial; Min/Max	**Signal Variance** θ Initial; Min/Max	α
$\mathcal{GP}_1$	10; [10, 10]	50^2; [50^2, 50^2]	10^{-10}
$\mathcal{GP}_2$	10; [1, 200]	50^2; [10^2, 100^2]	10

IV. Results and Discussion

A. Simulation Setup

The simulation studies are performed using Intel(R) Xeon(R) E-2144G CPU @ 3.60GHz. The OCPs of both control schemes are implemented in Python using CasADi 3.5.5 [17] and IPOPT 3.12.3 [18].

For the case studies, we perform simulation scenarios of 48 h (2 days), we set the prediction horizon to $N = 48$ and for the standard deviation prediction to $N_1 = 16$. The step size is set to $\delta_t = 0.25$ h.

To sample realizations of $\mathcal{Q}_{\text{dem}}$ and to forecast the resulting disturbances, we employ a separate GP for each. For the different scenarios, we sample 30 $\mathcal{Q}_{\text{dem}}$ realizations from $\mathcal{GP}_1$. The prior mean function is obtained by linearly interpolated, historical hourly data of seven days from [12]. For the subsequent forecasting of $\mathcal{Q}_{\text{dem}}$, cf. Remark 1, we utilize $\mathcal{GP}_2$, with the same prior mean and train it within each time step for the last $n_{obs} = 96$ observation points. The GPs are numerically implemented using the scikit-learn library [19] in Python. We choose squared exponential kernels, each consisting of a Radial Basis Function (RBF) kernel and a constant kernel. The initial values, training ranges of the hyperparameters and the value for α which defines the noise level in the targets, can be found in Table III. The forecasts of the prices which enter the stage cost in (17a), the power demand $\mathcal{P}_{\text{dem}}$, and PV supply are assumed to be exactly known. For that, we use the same realizations as those illustrated in the case studies in [4].

Table IV provides the parameters configured for the model- and data-driven OCPs and Table V gives an overview of the initial values and constraints for the operation of the simulation studies. To obtain the input-output pair of initial values for the data-driven predictive control and to ensure that both control schemes have the same starting conditions, we apply the initial control for one time step δ_t. Afterwards, the respective control scheme is started. For the first computation of the OCP, all initial values are set to zero. Afterwards, a warm start is performed at each control instant by initializing with computed trajectories from the previous iteration.

We construct the Hankel matrices for the data-driven system representation by sampled input trajectories from a uniform random distribution and the corresponding outputs. The considered output data is subject to noise with a signal-to-noise ratio of 26.99 dB. Table V provides the operation ranges of the sampled inputs. In order to enhance the prediction accuracy of the CHP dynamics, we set a minimum value for the sampled CHP inputs to 700 kW.

TABLE IV
Parameters

Parameter	Value	Parameter	Value	Parameter	Value
γ_{CHP}	$1 \cdot 10^{-5}$	ϵ	0.05	λ_g	10
γ_{BO}	$3 \cdot 10^{-5}$	λ_s	$1 \cdot 10^5$	λ_μ	$1 \cdot 10^5$
γ_{TES}	$9 \cdot 10^{-5}$				

TABLE V
Initial values and constraints

Variable	Initial Value	Min/Max	Variable	Initial Value	Min/Max
$\mathcal{Q}^{\text{in}}_{\text{CHP}}$	700	$[0, 1000]$	λ_{BO}	0.3	–
λ_{CHP}	0.8	–	$\mathcal{Q}_{\text{TES}}$	50	$[-100, 100]$
$\mathcal{Q}^{\text{out}}_{\text{CHP}}$	–	$[235, -]$	$\mathcal{E}_{\text{TES}}$	50	$[10, 140]$
$\mathcal{Q}^{\text{in}}_{\text{BO}}$	200	$[0, 300]$	$\mathcal{P}^{\text{in}}_{\text{EG}}/\mathcal{P}^{\text{out}}_{\text{EG}}$	–	$[0, 1000]$

B. Numerical Case Studies

In order to compare the proposed schemes with respect to performance and computation time, we perform 30 simulation studies for both schemes. For the following illustrations, we plot one scenario opaque to emphasize a coherent, overall operation while we visualize other scenarios in transparent colors. For the sake of visualization, various realizations of $\mathcal{Q}_{\text{dem}}$ are illustrated in Figure 2.

Figure 3 compares the model-based operation with the data-driven predictive control by depicting the inputs, states and outputs of CHP, boiler and TES. Accordingly to various $\mathcal{Q}_{\text{dem}}$ realizations in Figure 2, the respective operations profiles are shown for the inputs and stored thermal energy.

Corresponding to the daily energy demand, we obtain a smooth and similarly oscillating behavior for all components over the two days. Predominantly in daily intervals, the operation of TES alternates between states of charging and discharging. Most of the energy is supplied by the CHP, which allows selling the surplus energy back to the grid. During demand peaks, the CHP is operated in full load and in between it decreases to part load. The operation behavior of the stochastic data-driven predictive control is similar to the model-based scheme, however, some differences can be recognized. Compared to the model-based operation, it is notable that the overall operation of the data-driven predictive control is characterized by small fluctuations. In addition, the CHP is operated less intensively, whereas the boiler is utilized slightly more.

Table VI provides a comparison of the simulation studies,

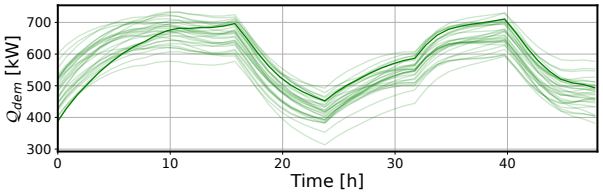

Fig. 2. Exogenous inputs: $\mathcal{Q}_{\text{dem}}$ realizations

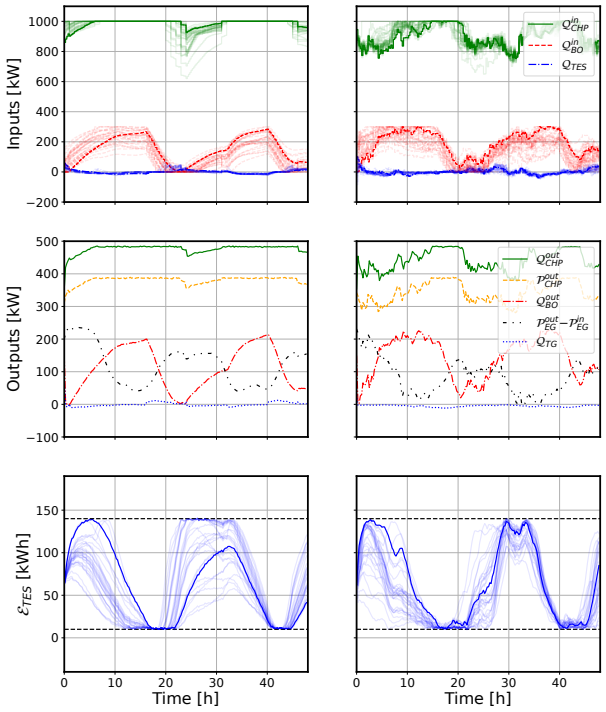

Fig. 3. Simulation results for stochastic model-based (left) and data-driven predictive control (right)

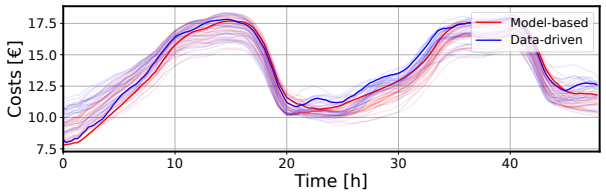

Fig. 4. Cost comparison - moving average of last 5 steps

including the number of decision variables $\#_d$, the computation time of OCPs, and operation costs of both schemes. We calculate the mean and standard deviation of the computation time from 5760 OCPs, resulting from the performed scenarios. Since the model-based uncertainty propagation scheme occurs outside the OCP, we take for the model-based scheme also the mean computation time and the standard deviation for the forward propagation into account. Hence, we can observe that the OCP solution of the data-driven scheme requires in total a 5.23 times higher computation time than the OCP solution and forward propagation of the model-based scheme, which can be explained by the larger number of decision variables. Nevertheless, with a step size of $\delta_t = 0.25\,\text{h}$, the data-driven scheme is still real-time capable and of interest for industrial applications. Evaluating the averaged total costs of the control schemes, we can observe that the operation of the data-driven scheme is approximately 1.76% more expensive than the model-based one.

C. Discussion

Data-driven uncertainty propagation stands out to be a promising method to quantify uncertainties within multi-

TABLE VI
Comparison of simulations
mean and SD of model-based forward propagation:
mean = $1.491 \cdot 10^{-3}s$ and SD = $4.493 \cdot 10^{-3}s$

Scheme	$\#_d$	Computation Time		Closed-loop Cost	
		Mean $[s]$	SD $[s]$	Mean [€]	SD [€]
Model-based	627	0.502	0.247	2600.77	97.16
Data-driven	6162	2.632	1.044	2646.42	101.67

energy systems without the requirement for extensive modelling burden. Analyzing the operation costs of the various operation scenarios, our simulation studies demonstrate that the stochastic data-driven predictive control performs similary as the model-based scheme. In contrast to the model-based uncertainty propagation with PCE, the data-driven scheme allows us to describe the nonlinear components with PCE coefficients and thus to account for uncertainties within the overall system. Due to the higher number of decision variables in the data-driven scheme, the computation time increases, but it still remains reasonable.

V. Conclusion

Uncertainties pose significant challenges for predictive control of multi-energy systems. The complexity of the arising models and the associated lack of system knowledge renders the quantification and propagation of uncertainties difficult. This paper has compared two different predictive control approaches in terms of operation performance and computation time. We considered a recently proposed stochastic data-driven approach that combines Willems' fundamental lemma with PCE to a simplified model-based predictive control scheme which also applies PCE in a pre-processing step. In contrast to the model-based scheme, the data-driven method considers uncertainties for the complete system and includes uncertainty propagation in the optimization problem without any further implementation effort. We demonstrated that the operational performance of the data-driven scheme is comparable with the model-based scheme. Although the computation time of the data-driven system is larger due to the increased problem size within the optimization, it is still real-time capable, which is interesting for the considered industrial applications. While modeling of complex real-world multi-energy systems poses a significant challenge for the application of model-based predictive control, the data-driven approach alleviates this bottleneck. Nonetheless in data-driven control, it is crucial to clarify the appropriate type and placement of sensors to obtain high-quality measurement data which in turn represents the system dynamics. The scalability of both methods heavily relies on the deployment of suitable hardware and software tools to foster implementation.

Future research should focus on tailoring numerical methods for fast computation of the data-driven predictive control and on creating forecasting methods which work with non-Gaussian distributions. In particular, the use of GPs entails the difficulty that the learned prediction model provides Gaussian random variables with unbounded support. In turn these are not truly realistic predictors for renewable energy sources which have limited operating ranges and thus implies compact support in random variable representations.

References

[1] Y. Zhou, Z. Ma, J. Zhang, and S. Zou, "Data-Driven Stochastic Energy Management of Multi Energy System using Deep Reinforcement Learning," *Energy*, vol. 261, p. 125187, 2022.

[2] T. M. Alabi, L. Lu, and Z. Yang, "Data-Driven Optimal Scheduling of Multi-Energy System Virtual Power Plant (MEVPP) Incorporating Carbon Capture System (CCS), Electric Vehicle Flexibility, and Clean Energy Marketer (CEM) Strategy," *Applied Energy*, vol. 314, p. 118997, 2022.

[3] J. C. Willems, P. Rapisarda, I. Markovsky, and B. L. De Moor, "A Note on Persistency of Excitation," *Systems & Control Letters*, vol. 54, no. 4, pp. 325–329, 2005.

[4] D. Bilgic, A. Koch, G. Pan, and T. Faulwasser, "Toward Data-driven Predictive Control of Multi-Energy Distribution Systems," *Electric Power Systems Research*, vol. 212, p. 108311, 2022.

[5] Y. Lian, J. Shi, M. Koch, and C. N. Jones, "Adaptive Robust Data-Driven Building Control via Bilevel Reformulation: An Experimental Result," *IEEE Transactions on Control Systems Technology*, vol. 31, no. 6, pp. 2420–2436, 2023.

[6] I. Markovsky and F. Dörfler, "Behavioral systems theory in data-driven analysis, signal processing, and control," *Annual Reviews in Control*, vol. 52, pp. 42–64, 2021.

[7] I. Markovsky, L. Huang, and F. Dörfler, "Data-driven control based on the behavioral approach: From theory to applications in power systems," *IEEE Control Systems Magazine*, vol. 43, no. 5, pp. 28–68, 2023.

[8] G. Pan, R. Ou, and T. Faulwasser, "On a Stochastic Fundamental Lemma and Its Use for Data-driven Optimal Control," *IEEE Transactions on Automatic Control*, vol. 68, no. 10, pp. 5922–5937, 2023.

[9] T. Mühlpfordt, T. Faulwasser, and V. Hagenmeyer, "A Generalized Framework for Chance-Constrained Optimal Power Flow," *Sustainable Energy, Grids and Networks*, vol. 16, pp. 231–242, 2018.

[10] T. Sullivan, *Introduction to Uncertainty Quantification*, ser. Texts in Applied Mathematics. Springer International Publishing, 2015.

[11] R. G. Ghanem and P. D. Spanos, *Stochastic Finite Elements: A Spectral Approach*. Courier Corporation, 2003.

[12] S. Sass, T. Faulwasser, D. E. Hollermann, C. D. Kappatou, D. Sauer, T. Schütz, D. Y. Shu, A. Bardow, L. Gröll, V. Hagenmeyer, D. Müller, and A. Mitsos, "Model Compendium, Data, and Optimization Benchmarks for Sector-Coupled Energy Systems," *Computers & Chemical Engineering*, vol. 135, p. 106760, 2020.

[13] M. Farina, L. Giulioni, L. Magni, and R. Scattolini, "A Probabilistic Approach to Model Predictive Control," in *52nd IEEE Conference on Decision and Control*, Dec 2013, pp. 7734–7739.

[14] J. Coulson, J. Lygeros, and F. Dörfler, "Data-enabled predictive control: In the shallows of the deepc," in *2019 18th European Control Conference (ECC)*, 2019, pp. 307–312.

[15] P. Zometa, H. Heinemann, S. Lucia, M. Kögel, and R. Findeisen, "Efficient Stochastic Model Predictive Control for Embedded Systems Based on Second-Order Cone Programs," in *2016 European Control Conference (ECC)*, 2016, pp. 166–171.

[16] G. Pan and T. Faulwasser, "Distributionally robust uncertainty quantification via data-driven stochastic optimal control," *IEEE Control Systems Letters*, vol. 7, pp. 3036–3041, 2023.

[17] J. A. E. Andersson, J. Gillis, G. Horn, J. B. Rawlings, and M. Diehl, "CasADi: a software framework for nonlinear optimization and optimal control," *Mathematical Programming Computation*, vol. 11, no. 1, pp. 1–36, Mar. 2019.

[18] A. Wächter and L. T. Biegler, "On the implementation of an interior-point filter line-search algorithm for large-scale nonlinear programming," *Mathematical programming*, vol. 106, pp. 25–57, 2006.

[19] F. Pedregosa, G. Varoquaux, A. Gramfort, V. Michel, B. Thirion, O. Grisel, M. Blondel, P. Prettenhofer, R. Weiss, V. Dubourg, J. Vanderplas, A. Passos, D. Cournapeau, M. Brucher, M. Perrot, and E. Duchesnay, "Scikit-Learn: Machine Learning in Python," *J. Mach. Learn. Res.*, vol. 12, no. null, p. 2825–2830, 2011.